Influence of strain on anisotropic thermoelectric transport in Bi_2Te_3 and Sb_2Te_3

N. F. Hinsche,[1,*] B. Yu. Yavorsky,[1] I. Mertig,[1,2] and P. Zahn[1]

[1]*Institut für Physik, Martin-Luther-Universität Halle-Wittenberg, DE-06099 Halle, Germany*

[2]*Max-Planck-Institut für Mikrostrukturphysik, Weinberg 2, DE-06120 Halle, Germany*

(Received 25 July 2011; revised manuscript received 14 October 2011; published 28 October 2011; publisher error corrected 13 February 2012)

On the basis of detailed first-principles calculations and semiclassical Boltzmann transport, the anisotropic thermoelectric transport properties of Bi_2Te_3 and Sb_2Te_3 under strain were investigated. It was found that due to compensation effects of the strain-dependent thermopower and electrical conductivity, the related power factor will decrease under applied in-plane strain for Bi_2Te_3, while being stable for Sb_2Te_3. A clear preference for thermoelectric transport under hole doping, as well as for the in-plane transport direction was found for both tellurides. In contrast to the electrical conductivity anisotropy, the anisotropy of the thermopower was almost robust under applied strain. The assumption of an anisotropic relaxation time for Bi_2Te_3 suggests that already in the single crystalline system strong anisotropic scattering effects should play a role.

DOI: 10.1103/PhysRevB.84.165214 PACS number(s): 31.15.A−, 71.15.Mb, 72.20.Pa

I. INTRODUCTION

Thermoelectric (TE) materials are used as solid-state energy devices that convert waste heat into electricity or electrical power directly into cooling or heating.[1–3] Telluride-based thermoelectrics, e.g., the bulk materials bismuth (Bi_2Te_3), antimony telluride (Sb_2Te_3), and their related alloys, dominate efficient TE energy conversion at room temperature for the last 60 years.[4,5] The materials TE efficiency is quantified by the figure of merit

$$ZT = \frac{\sigma S^2}{\kappa_{el} + \kappa_{ph}} T, \tag{1}$$

where σ is the electrical conductivity, S the thermopower, κ_{el} and κ_{ph} are the electronic and phononic contributions to the thermal conductivity, respectively. From Eq. (1) it is obvious that a higher ZT is obtained by decreasing the denominator or by increasing the numerator, the latter being called the power factor $PF = \sigma S^2$. While bulk $Bi_2Te_3$and Sb_2Te_3 show ZT values smaller than one and applications have been limited to niche areas, a breaktrough experiment of Venkatasubramanian *et al.* showed a remarkable $ZT = 2.4/1.5$ for *p*-type/*n*-type superlattices (SLs) composed of the two bulk tellurides.[5–7] With the availability of high-ZT materials, many new applications will emerge.[2] The idea of thermoelectric SL follows the idea of phonon blocking and electron transmitting at the same time. It suggests that cross-plane transport along the direction perpendicular to the artificial interfaces of the SL reduces phonon heat conduction while maintaining or even enhancing the electron transport.[3] While some effort in experimental research was done,[8–13] only a few theoretical works discuss the possible transport across such SL structures.[14,15] While Park *et al.*[14] discussed the effect of volume change on the in-plane thermoelectric transport properties of Bi_2Te_3, Sb_2Te_3, and their related compounds, Li *et al.*[15] focussed on the calculation of the electronic structure for a Bi_2Te_3/Sb_2Te_3 SL, stating changes of the mobility anisotropy estimated from effective masses.

Superlattices are anisotropic by definition and even the telluride bulk materials show intrinsic anisotropic structural and electronic properties. However, investigations of Venkatasubramanian *et al.* found a strong decrease for the mobility anisotropy and the thermoelectric properties for the Bi_2Te_3/Sb_2Te_3 SLs at certain periods. The reason for this behavior is still under debate and could be related to strain effects, which are induced by the epitaxial growth of the Bi_2Te_3/Sb_2Te_3 SLs. To extend previous works[16–18] and to clarify the open question on the reduced anisotropy, we are going to discuss in this paper the anisotropic electronic transport in bulk Bi_2Te_3 and Sb_2Te_3 and the possible influence of strain in epitaxially grown SL on the TE properties.

For this purpose, the paper will be organized as follows. In Sect. II, we introduce our first-principles electronic structure calculations based on density functional theory and the semiclassical transport calculations based on the solution of the linearized Boltzmann equation. With this, we discuss the thermoelectric transport properties, that is, electrical conductivity, thermopower, and the related power factor of unstrained Bi_2Te_3 and $Sb_2Te_3$with a focus on their directional anisotropies. While in epitaxially grown the atoms near the interfaces may be shifted from their bulk positions due to the lattice mismatch and the changed local environment, we modeled Bi_2Te_3 with the experimental lattice parameters and interatomic distances of Sb_2Te_3 and vice versa. We assume that from these two limiting cases, one could estimate the effect of the interface relaxation on the electronic and transport properties in Bi_2Te_3/Sb_2Te_3 SLs. With these structural data we first analyze in Sec. III, the anisotropic thermoelectric properties of the unstrained bulk systems, while in Sec. IV, a detailed view on the influence of strain, which may occur in Bi_2Te_3/Sb_2Te_3 SLs, on the electronic transport of these tellurides is given. Throughout the paper we quote $Bi_2Te_3(Sb_2Te_3)$ as strained, if it is considered in the lattice structure of $Sb_2Te_3(Bi_2Te_3)$. As in the SL, *p* type as well as *n* type transport was reported, we discuss the concentration dependence for both types of carriers on the transport properties.

II. METHODOLOGY

For both bismuth and antimony telluride, we used the experimental lattice parameters and relaxed atomic positions[19] as provided for the rhombohedral crystal structure with five

 ©2011 American Physical Society

atoms, i.e., one formula unit, per unit cell belonging to the space group D_{3d}^5 ($R\bar{3}m$). The related layered hexagonal structure is composed out of three formula units and has the lattice parameters $a_{\mathrm{BiTe}}^{\mathrm{hex}} = 4.384$ Å, $c_{\mathrm{BiTe}}^{\mathrm{hex}} = 30.487$ Å, and $a_{\mathrm{SbTe}}^{\mathrm{hex}} = 4.264$ Å, $c_{\mathrm{SbTe}}^{\mathrm{hex}} = 30.458$ Å, for Bi_2Te_3 and Sb_2Te_3, respectively. In fact, the main difference between the lattices of Bi_2Te_3 and Sb_2Te_3 is a decrease of the in-plane lattice constant with an accompanied decrease in the cell volume. So, a change between the two lattice constants can be related to either compressive or tensile in-plane strain. This is very similar to the approach by Park *et al.*[14] while omitting computational relaxation of internal atomic positions.

Our electronic structure calculations are performed in two steps. In a first step, the detailed band structures of the strained and unstrained $Bi_2Te_3$and Sb_2Te_3 were obtained (see Fig. 1) by first-principles density functional theory calculations (DFT), as implemented in the fully relativistic screened Korringa-Kohn-Rostoker Greens-function method (KKR).[20] Within this approach, the Dirac equation is solved self-consistently and with the spin-orbit coupling included. Exchange and correlation effects were accounted for by the local density approximation (LDA) parametrized by Vosco, Wilk, and Nusair.[21] A detailed discussion on the influence of strain on the band structure topology of Bi_2Te_3 and Sb_2Te_3 is recently published.[22]

With the well-converged results from the first step, we obtain the thermoelectric transport properties by solving the linearized Boltzmann equation in relaxation time approximation (RTA) within an in-house developed Boltzmann transport code.[23–25] Boltzmann transport calculations for thermoelectrics have been carried out for quite a long time and show reliable results for metals[26–28] as well as for wide- and narrow-gap semiconductors.[25,29–32] TE transport calculations for bulk Bi_2Te_3[14,18,33,34] and Sb_2Te_3[14,17,35] were presented before. Here, the relaxation time τ is assumed to be constant with respect to wave vector k and energy on the scale of $k_B T$. This assumption is widely accepted for metals and highly doped semiconductors. Most of the presented results are in this high-doping regime. Within the RTA, the transport distribution function $\mathcal{L}_{\perp,\parallel}^{(0)}(\mu,0)$ (TDF)[36] and with this the generalized conductance moments $\mathcal{L}_{\perp,\parallel}^{(n)}(\mu,T)$ are defined as

$$\mathcal{L}_{\perp,\parallel}^{(n)}(\mu,T) = \frac{\tau_{\parallel,\perp}}{(2\pi)^3} \sum_{\nu} \int d^3k \left(v_{k,(\perp,\parallel)}^{\nu}\right)^2 \times \left(E_k^{\nu} - \mu\right)^n \left(-\frac{\partial f_{(\mu,T)}}{\partial E}\right)_{E=E_k^{\nu}}. \quad (2)$$

$v_{k,(\parallel)}^{\nu}$ and $v_{k,(\perp)}^{\nu}$ denote the group velocities in the directions in the hexagonal basal plane and perpendicular to it, respectively. Within, the group velocities were obtained as derivatives along the lines of the Blöchl mesh in the whole Brillouin zone.[22] A detailed discussion on implications and difficulties of the numerical determination of the group velocities in highly anisotropic materials is currently published elsewhere.[37] As can be seen straightforwardly, the in- and cross-plane electrical conductivity σ is then given by

$$\sigma_{\perp,\parallel} = 2e^2 \mathcal{L}_{\perp,\parallel}^{(0)}(\mu,T) \quad (3)$$

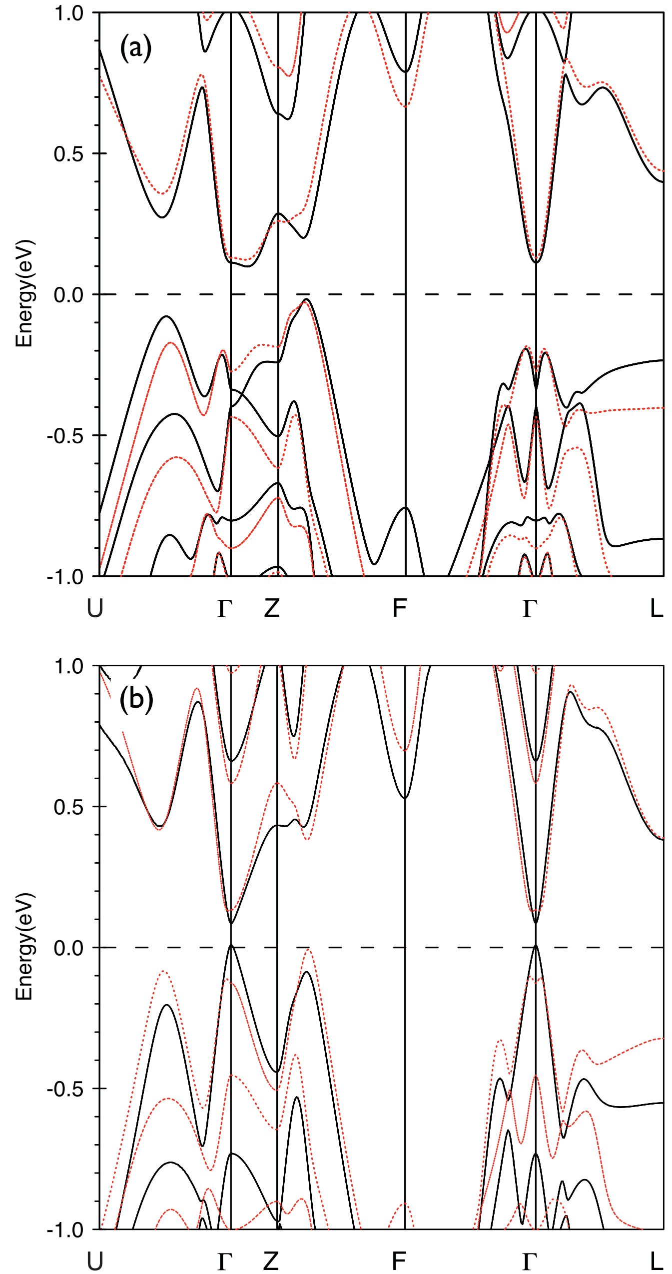

FIG. 1. (Color online) Band structures of (a) Bi_2Te_3 and (b) Sb_2Te_3 along symmetry lines for both unstrained (black solid lines) and strained (red dashed lines) lattices. Energies are given relative to the valence band maximum.

and the temperature- and doping-dependent thermopower states as

$$S_{\perp,\parallel} = \frac{1}{eT} \frac{\mathcal{L}_{\perp,\parallel}^{(1)}(\mu,T)}{\mathcal{L}_{\perp,\parallel}^{(0)}(\mu,T)} \quad (4)$$

for given chemical potential μ at temperature T and extrinsic carrier concentration N determined by an integration over the density of states $n(E)$:

$$N = \int_{\mu-\Delta E}^{\mathrm{VB^{max}}} dE\, n(E)[f_{(\mu,T)} - 1] + \int_{\mathrm{CB^{min}}}^{\mu+\Delta E} dE\, n(E) f_{(\mu,T)}, \quad (5)$$

where CB^{min} is the conduction band minimum and VB^{max} is the valence band maximum (VBM). The energy range ΔE has to be taken sufficiently large to cover the tails of the Fermi-Dirac distribution function $f_{(\mu,T)}$ and to ensure convergence of the integrals in Eqs. (2) and (5).[25] The k-space integration of Eq. (2) for a system with an intrinsic anisotropic texture is quite demanding. In previous publications,[22,37] we stated on the relevance of adaptive integration methods needed to reach convergence of the energy-dependent TDF. Especially in regions close to the band edges, the anisotropy of the TDF requires a high density of the k mesh. Here, convergence tests for the transport properties showed that at least 150 000 k points in the entire BZ had to be included for sufficient high doping rates ($N \geqslant 1 \times 10^{19}$ cm^{-3}), while for energies near the band edges, even more than 56 million k points were required to reach the analytical values for the conductivity anisotropies at the band edges. (The analytical value of the ratio $\sigma_{\parallel}/\sigma_{\perp}$ at the band edges was obtained by scanning the energy landscape near the conduction band minimum and valence band maximum fitting the dispersion relation in terms of an effective mass tensor. A detailed description is given in a recent publication by Ref. 22.) Within the RTA, from comparison of the calculated electrical conductivities [Eq. (3)] with experiment it is possible to conclude on the directional anisotropy of τ. For the thermopower S [Eq. (4)], the dependence of the TDF on the energy is essential. That is, not only the slope of the TDF, moreover, the overall functional behavior of the TDF on the considered energy scale has to change to observe an impact on the thermopower. The calculations in this paper aim to cover band structure effects and not scattering-specific impacts by an energy- and state-dependent relaxation time.

III. ANISOTROPIC THERMOELECTRIC PROPERTIES OF UNSTRAINED Bi_2Te_3 AND Sb_2Te_3

In order to understand the experimental findings on the in-plane and cross-plane transport of the Bi_2Te_3/Sb_2Te_3 SLs, in the following section, the anisotropies of the electrical conductivity, the thermopower, and the related power factor of bulk Bi_2Te_3 and Sb_2Te_3 are discussed. Even though the behavior of Sb_2Te_3 is strongly p type with an extrinsic carrier concentration of $N = 1$–10×10^{20} cm^{-3},[38] we also discuss the related n-doped case, as in Bi_2Te_3/Sb_2Te_3 SLs, n as well as p dopings were reported. Bulk Bi_2Te_3 is known to be inherent electron conducting, while hole doping is experimentally achievable for bulk systems.[4,39–41]

Figure 2 shows the variation of the anisotropic thermopower for unstrained Bi_2Te_3 and Sb_2Te_3 in a wide temperature range. The extrinsic charge carrier concentration of Bi_2Te_3 and Sb_2Te_3 was fixed to $N = 1 \times 10^{19}$ cm^{-3} and $N = 1 \times 10^{20}$ cm^{-3}, respectively. As a reference, experimental values for both single crystalline materials at the same doping conditions are given and an excellent agreement can be stated. It is worth noting that within Eq. (4), the calculation of the thermopower is completely free of parameters. For Bi_2Te_3, the in-plane thermopower reaches a maximum of $S_{\parallel} \sim -200\,\mu$V/K at 300 K, while the maximum for the hole-doped case is shifted to slightly higher temperatures of 350 K with a maximum value of $S_{\parallel} \sim 225\,\mu$V/K. We note,

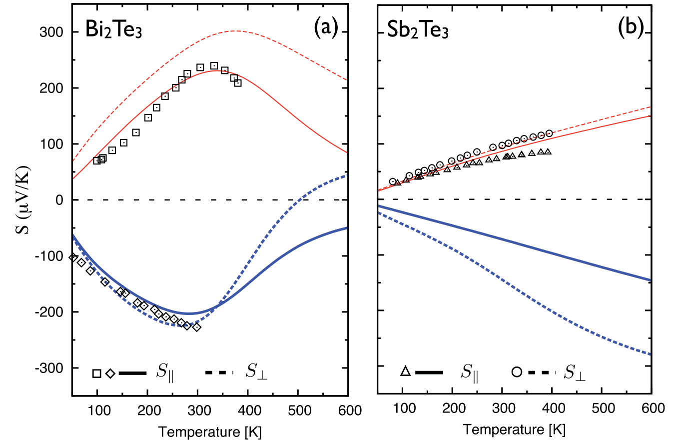

FIG. 2. (Color online) Anisotropic thermopower for bulk (a) Bi_2Te_3 and (b) Sb_2Te_3 in their unstrained bulk lattice constants. Electron doping refers to the blue (thick) lines in the lower part of the figure, while red (thin) lines refer to hole doping and positive values of the thermopower. Solid lines show the in-plane part $S_{\parallel}$ of the thermopower, while dashed lines show the cross-plane part $S_{\perp}$. The extrinsic charge carrier concentration of Bi_2Te_3 and Sb_2Te_3 was fixed to $N = 1 \times 10^{19}$ cm^{-3} and $N = 1 \times 10^{20}$ cm^{-3}, respectively. Experimental data (squares, diamonds, circles, triangles) from Refs. 41–43 are given for comparison.

that the temperature of the maximum is slightly overestimated. This might be caused by the missing temperature dependence of the energy gap, which was determined as $E_g = 105$ meV for unstrained Bi_2Te_3. The anisotropy of the thermopower is more pronounced for the p-doped case. Here, the cross-plane thermopower $S_{\perp}$ is, for the given doping, always larger than the in-plane part $S_{\parallel}$. The anisotropy $\frac{S_{\parallel}}{S_{\perp}}$ is about 0.64 at 100 K, evolving to $S_{\parallel}/S_{\perp} \sim 0.79$ and $S_{\parallel}/S_{\perp} \sim 0.55$ at 300 and 500 K, respectively. The sole available experimental data show no noticeable anisotropy for the thermopower in the hole-doped case.[42] For the electron-doped case, the situation is more sophisticated. While up to 340 K the overall anisotropy is rather small, with values $S_{\parallel}/S_{\perp} \sim 0.9$, a considerable decrease of $S_{\perp}$ at higher temperatures leads to high values of $S_{\parallel}/S_{\perp}$ for temperatures above 400 K. This tendency could also be revealed by experiments.[44,45] The crossing point of $S_{\parallel}$ and $S_{\perp}$ near room temperature could explain the fact of varying measured anisotropies for the thermopower at 300 K. Here, anisotropy ratios of $S_{\parallel}/S_{\perp} = 0.97$–$1.10$ were reported.[41,45] The maximum peak of the thermopower near room temperature can be explained by the position of the chemical potential μ as a function of temperature at a fixed carrier concentration. For T much smaller than 300 K, the chemical potential is located in either the conduction or valence band with the tails of the Fermi-Dirac distribution in Eq. (2) only playing a subsidiary role. For rising temperatures, the chemical potential shifts toward the band edges, and S maximizes. At these conditions, the conduction is mainly unipolar. For higher temperatures, the chemical potential shifts into the band gap and conduction becomes bipolar leading to a reduced thermopower. For the case of Sb_2Te_3, shown in Fig. 2(b), the situation is different. Due to the ten-times-higher inherent doping and the smaller energy gap of

$E_g = 90$ meV, the chemical potential is located deeply in the bands for the whole relevant temperature range. Therefore the functional behavior can be understood in terms of the well-known Mott relation, where Eq. (4) qualitatively coincides with $S \propto T \frac{d \ln \sigma(E)}{dE}|_{E=\mu}$ for the thermopower in RTA.[46] With increasing temperature, the thermopower increases almost linearly, showing values of $S_{\parallel} \sim 87\ \mu$V/K and $S_{\parallel} \sim -72\ \mu$V/K at 300 K for p and n doping, respectively. The anisotropy of the thermopower for the hole-doped case is around $S_{\parallel}/S_{\perp} = 0.91$, almost temperature independent and slightly underestimates the available experimental values.[47,48] While for the electron-doped case the absolute values of the in-plane thermopower are comparable to those of the hole-doped case, the anisotropies are rather large. The anisotropy varies only weakly on temperature, showing $S_{\parallel}/S_{\perp} = 0.48$–$0.52$ over the hole temperature range. While bulk Sb_2Te_3 states have a strong p character due to inherent defects, we note here again, that n doping is available in heterostructures combining Bi_2Te_3 and Sb_2Te_3.[5]

A strongly enhanced cross-plane thermopower $S_{\perp}$ could lead to a strongly enhanced power factor $\mathrm{PF}_{\perp}$, if the cross-plane electrical conductivity $\sigma_{\perp}$ is maintained at the bulk value.

For this purpose, the anisotropy of the electrical conductivity in dependence on the in-plane conductivity $\sigma_{\parallel}$ for unstrained Bi_2Te_3 and Sb_2Te_3 is shown in Fig. 3. The temperature is fixed at 300 K, blue and red lines refer to electron and hole doping, respectively. From comparison with experimental data, the in-plane relaxation time is determined to be $\tau_{\parallel} = 1.1 \times 10^{-14}$ and 1.2×10^{-14} s for Bi_2Te_3 and Sb_2Te_3, respectively. (The calculated dependencies of the electrical conductivity on the thermopower and on the applied doping were matched to fit experiments from Refs. 4, 39, and 48.) With that, we find strong anisotropies for the electrical conductivity $\sigma_{\parallel}/\sigma_{\perp} \gg 1$, clearly preferring the in-plane transport in both bulk tellurides. For the strongly suppressed cross-plane conduction, p-type conduction is more favored than n type. For Bi_2Te_3, the pure band structure effects [solid lines in Fig. 3(a)] overestimate the measured anisotropy ratio[39] of the electrical conductivity. With an assumed anisotropy of the relaxation time of $\tau_{\parallel}/\tau_{\perp} = 0.47$, the experimental values are reproduced very well. This means that scattering effects strongly affect the transport, and electrons traveling along the basal plane direction are scattered stronger than electrons traveling perpendicular to the basal plane. The origin of this assumed anisotropy has to be examined by defect calculations, resulting microscopic transition probabilities, and state-dependent mean free path vectors. It is well known that in Bi_2Te_3, mainly antisite defects lead to the inherent conduction behavior.[38,45,50] We have shown elsewhere[37] that the integration of the transport integrals (2) in anisotropic k space requires large numerical effort. Tiny regions in k space close to the band gap have to be scanned very carefully, and the texture in k space has a drastic influence on the obtained anisotropy values, if integrals are not converged with respect to the k-point density. As shown, some integration methods tend for the given k-space symmetry to underestimate the ratio $\sigma_{\parallel}/\sigma_{\perp}$ in a systematic manner, and therefore would shift anisotropy closer to the experimental observed values, without representing the real

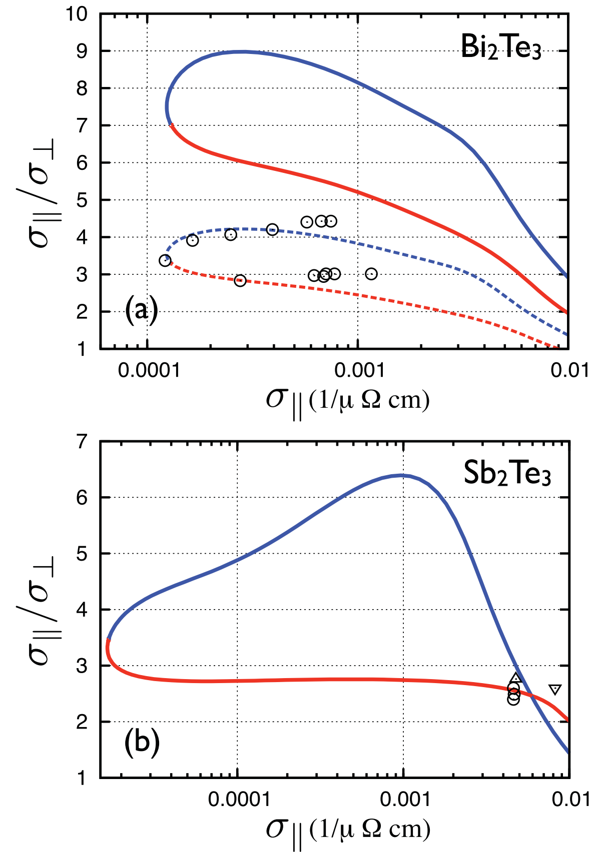

FIG. 3. (Color online) Ratio $\sigma_{\parallel}/\sigma_{\perp}$ of the electrical conductivites at 300 K for unstrained bulk (a) Bi_2Te_3 and (b) Sb_2Te_3. Electron doping refers to blue lines, while red lines refer to hole doping. The dashed lines in panel (a) present the ratio obtained with an anisotropic relaxation time $\tau_{xx}/\tau_{zz} = 0.47$, while all other results are obtained with an isotropic relaxation time. Experimental data (circles and triangles) from Refs. 39, 49, and 48 are given for comparison.

band structure effects. For unstrained Bi_2Te_3, the electrical conductivity anisotropy is the highest for low values of $\sigma_{\parallel}$, i.e., small amounts of doping and bipolar conduction. For larger charge carrier concentrations, i.e., the chemical potential shifts deeper into either conduction or valence band, the in-plane conductivity $\sigma_{\parallel}$ increases and the ratio $\sigma_{\parallel}/\sigma_{\perp}$ decreases. Values for $\sigma_{\parallel}/\sigma_{\perp}$ will lower from seven to two for p-type conduction and nine to three for n-type conduction. However, cross-plane electrical transport is always more suppressed for n-type carrier conduction, which also holds for unstrained Sb_2Te_3. As shown in Fig. 3(b), $\sigma_{\parallel}/\sigma_{\perp}$ is almost doping independent for hole doping, showing an anisotropy of around 2.7 in very good agreement with experiment (circle and triangles in Fig. 3 from Refs. 47–49). In this case, no anisotropic relaxation times had to be assumed. For electron doping, the ratio $\sigma_{\parallel}/\sigma_{\perp}$ is clearly higher, evolving values of 3.5 to 6 for rising in-plane conductivity. The dependence of the anisotropy ratio on the applied doping, i.e., changing $\sigma_{\parallel}$, can be directly linked to the functional behaviour of the TDF near band edges, which is crucially influenced by the topology of the band structure.[22]

IV. ANISOTROPIC THERMOELECTRIC PROPERTIES OF STRAINED Bi_2Te_3 AND Sb_2Te_3

Before the influence of in-plane strain on the resulting power factor will be discussed, we will first note on the strain-induced changes of the components electrical conductivity and thermopower. In Fig. 4, the anisotropy of the electrical conductivity $\sigma_\parallel/\sigma_\perp$ is shown for both Bi_2Te_3 in the lattice constant of Sb_2Te_3, i.e., under biaxial compressive in-plane strain [Fig. 4(a)], and Sb_2Te_3 in the lattice constant of Bi_2Te_3, i.e., under biaxial tensile in-plane strain [Fig. 4(b)].

For Bi_2Te_3, the compressive in-plane strain causes an increase of the the band gap by around 23% yielding $E_g = 129$ meV. While the anisotropy $\sigma_\parallel/\sigma_\perp$ for hole doping [red lines in Fig. 4(a)] decreases to around four and is almost constant under varying doping level, the ratio rises considerably under electron doping to values up to 13 for $\sigma_\parallel \sim 100$–$1000\ (\Omega\,\mathrm{cm})^{-1}$, corresponding to electron charge carrier concentrations of $N = 3$–30×10^{19} cm^{-3}. This concludes, that the cross-plane electrical conductivity of Bi_2Te_3 under compressive in-plane strain will be noticeably enhanced for p doping, but drastically suppressed for n doping. Such a compressive in-plane strain could be introduced by either a substrate with smaller in-plane lattice constant, e.g.,

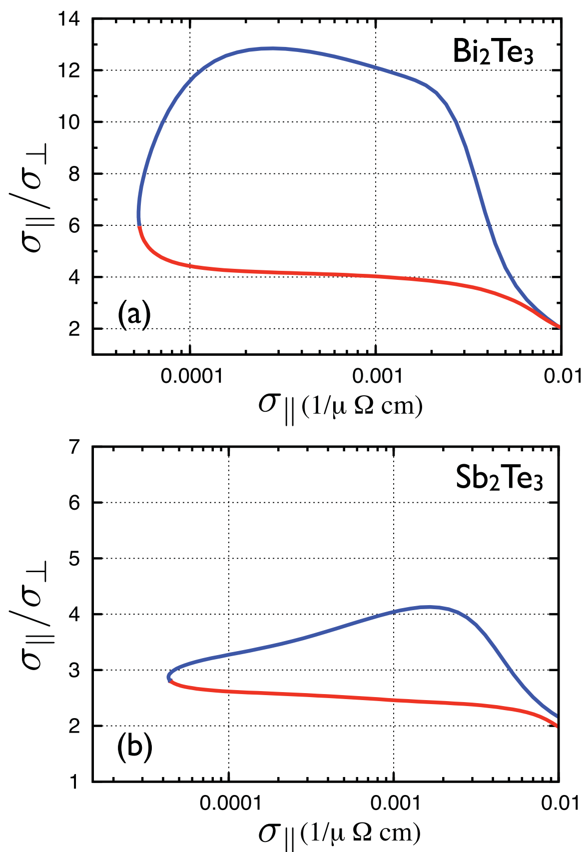

FIG. 4. (Color online) Conductivity ratio $\sigma_\parallel/\sigma_\perp$ of the electrical conductivites at 300 K for bulk (a) Bi_2Te_3 in the Sb_2Te_3 structure and (b) Sb_2Te_3 in the Bi_2Te_3 structure. Electron doping refers to blue lines, while red lines refer to hole doping. Isotropic relaxation times of $\tau = 1.1 \times 10^{-14}$ and 1.2×10^{-14} s for $\sigma_\parallel$ and $\sigma_\perp$ are assumed for Bi_2Te_3 and Sb_2Te_3, respectively.

GaAs-[111] with $a = 3.997$ Å, or by a considerable amount of Sb_2Te_3 in the Bi_2Te_3/Sb_2Te_3 SLs. For tensile in-plane strained Sb_2Te_3, the impact on the electrical conductivity ratio $\sigma_\parallel/\sigma_\perp$ is less prominent. As shown in Fig. 4(b), at hole doping, $\sigma_\parallel/\sigma_\perp \sim 2.5$ is only marginally altered compared to the unstrained case [compare Fig. 3(b)]. Meanwhile $\sigma_\parallel/\sigma_\perp$ decreases noticeably for n-type doping yielding about three at low $\sigma_\parallel$ and low electron charge carrier concentrations, and slightly higher values of $\sigma_\parallel/\sigma_\perp \sim 4$ for higher doping. Overall, the tensile strain reduces the electrical conductivity anisotropy by a factor of about 1.5, directly leading to an enhanced electrical conductivity along the z axis of single-crystal Sb_2Te_3. We note that tensile in-plane strain opens the gap remarkably by around 56% compared to the unstrained case to a value of $E_g = 140$ meV. Furthermore, such tensile strain could be incorporated by using either a substrate with larger in-plane lattice constant, e.g., PbTe-[111] with $a = 4.567$ Å, or a higher fractional amount of Bi_2Te_3 in Bi_2Te_3/Sb_2Te_3 SLs.

In Fig. 5(a) and 5(d) [5(b) and 5(c)], the doping-dependent anisotropic thermopower of unstrained (strained) Bi_2Te_3 and Sb_2Te_3 at room temperature are shown, respectively. Blue thick (red thin) solid lines represent the in-plane thermopower $S_\parallel$ under electron doping (hole doping). The corresponding cross-plane thermopower $S_\perp$ is shown as a dashed line. The black dashed-dotted lines in Fig. 5(d) emphasize the expected doping-dependent behavior of the thermopower for parabolic bands, following the Pisarenko relation.[52] For both tellurides, we found that the anisotropy of the thermopower shows a weak dependence on the strain state. However, for strained Bi_2Te_3 [see Fig. 5(b)], the thermopower anisotropy under hole doping almost vanishes, leading to $S_\parallel \sim S_\perp$. It is worth noting that the anisotropy of the thermopower is less pronounced for hole doping, than for electron doping for Bi_2Te_3 and Sb_2Te_3 in both strain states. As shown by the black dashed-dotted lines in Fig. 5(d), the dependence of the thermopower on the charge carrier concentration differs from the Pisarenko relation[52] under sufficient high electron doping. This indicates that the nonparabolicity of the energy bands has a noticeable impact in the investigated doping regime and should not be omitted by applying parabolic band models.

Actually, changes for the absolute values of the thermopower can be found for both telluride systems under applied strain. In Fig. 6, the relative change for the in-plane component $S_\parallel$ for both tellurides under in-plane strain is given. To compare the changes with the lattice constant, we relate the in-plane thermopower $S_\parallel$ at the smaller lattice constant a_{SbTe} to the value at the larger lattice constant a_{BiTe} for both compounds. The doping was fixed to $N = 1 \times 10^{19}$ cm^{-3} for Bi_2Te_3 and $N = 1 \times 10^{20}$ cm^{-3} for Sb_2Te_3 as done for Fig. 2. Figure 6(a) shows that in the relevant temperature range between 350 and 450 K, the thermopower increases for Bi_2Te_3 under compressive strain for both p and n doping by about 15–20%. For Sb_2Te_3, a decrease is expected under tensile strain at electron doping and nearly no change under hole doping [see Fig. 6(b)]. With nearly all values above one for Bi_2Te_3 as well as for Sb_2Te_3 it is obvious that higher values of the thermopower require a smaller unit cell volume. One can expect that the volume decrease causes a larger density of states and thus a shift of the chemical potential toward the corresponding band edge, connected with an increase of the thermopower S.

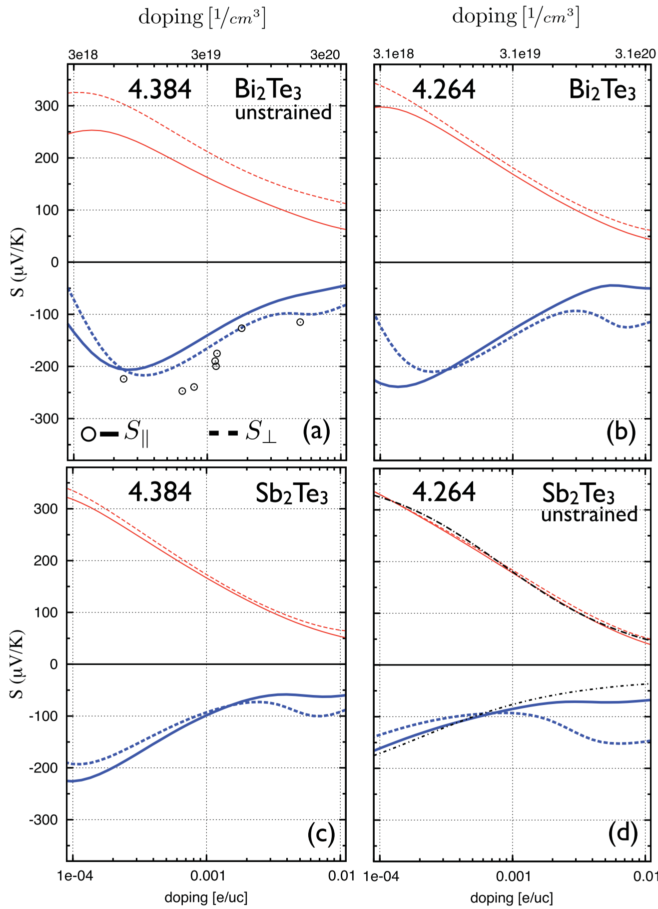

FIG. 5. (Color online) In-plane (solid lines) and cross-plane (dashed lines) doping-dependent thermopower at 300 K for (a) Bi_2Te_3 in the Bi_2Te_3, (b) Bi_2Te_3 in the Sb_2Te_3, (c) Sb_2Te_3 in the Bi_2Te_3, and (d) Sb_2Te_3 in the Sb_2Te_3 structures. Electron (hole) doping is presented as blue thick (red thin) line. The black (dashed-dotted) line in panel (d) shows the Pisarenko dependence of the thermopower expected for parabolic bands. Experimental data (circles) from Ref. 51 are given for comparison. The charge carrier concentration is stated in units of electron per unit cell (e/uc) ($1/cm^3$) at the bottom (top) x axis.

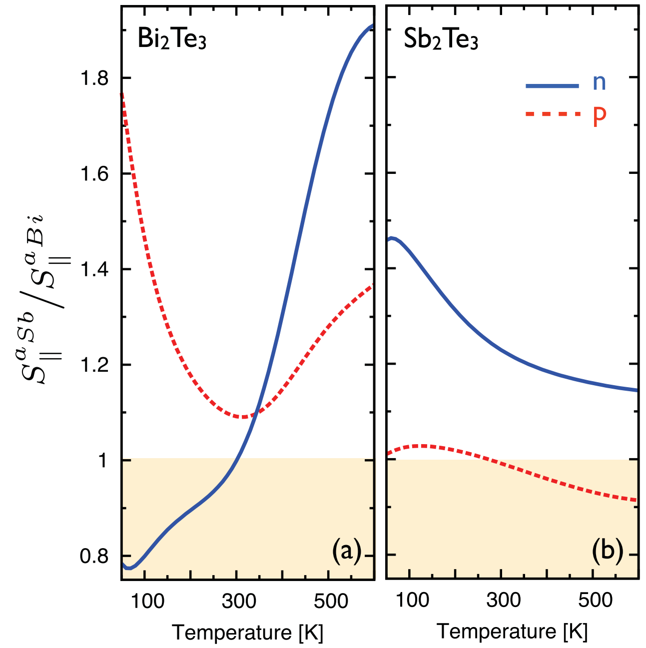

FIG. 6. (Color online) Change of the in-plane thermopower $S_\parallel$ under applied strain for (a) Bi_2Te_3 and (b) Sb_2Te_3. Given is the ratio of $S_\parallel$ in the "smaller" lattice of Sb_2Te_3 divided by $S_\parallel$ in the "larger" lattice of Bi_2Te_3. The doping was fixed to $N = 1 \times 10^{19}$ cm^{-3} for Bi_2Te_3 and $N = 1 \times 10^{20}$ cm^{-3} for Sb_2Te_3. Solid blue (dashed red) lines refer to electron (hole) doping, respectively.

However, Park *et al.*[14] reported an unexpected increase of 16% for the in-plane thermopower $S_\parallel$ of Sb_2Te_3 under p doping ($T = 300$ K and $N = 1.32 \times 10^{19}$ cm^{-3}) if the material is strained into the Bi_2Te_3 structure. In the same doping and temperature regime, we find a slight decrease of 4% for $S_\parallel$.

Comprising the statements on the electrical conductivity and the thermopower, the related power factor for both tellurides in their bulk lattice and in the strained state are compared in Fig. 7. It is well known that optimizing the power factor σS^2 of a thermoelectric always involves a compromise on the electrical conductivity σ and the thermopower S.[53] Due to the interdependence of σ and S, it is not advisable to optimize the power factor by optimizing its parts.

In Figs. 7(a) and 7(d), the doping-dependent anisotropic power factor of unstrained Bi_2Te_3 and Sb_2Te_3 at room temperature is shown, respectively. Blue thick (red thin) solid lines represent the in-plane power factor $PF_\parallel$ under electron doping (hole doping). The corresponding cross-plane power factor $PF_\perp$ is shown as a dashed line. Under p doping, both unstrained materials show a maximum power factor near carrier concentrations of $N \sim 4 \times 10^{19}$ cm^{-3}. Absolute values of 35 and 33 μW/cm K^2 were found for unstrained Bi_2Te_3 and Sb_2Te_3, respectively, which is in good agreement with experimental and theoretical findings.[9,14,51] Under electron doping, the absolute values of $PF_\parallel$ (thick blue lines in Fig. 7) were found to be distinctly smaller. This is due to smaller absolute values of the thermopower for electron doping compared to hole doping (see Fig. 2) and apparently smaller in-plane electrical conductivities $\sigma_\parallel$ at fixed carrier concentrations. As a result, a power factor of 18 and 8 μW/cm K^2 can be stated for unstrained Bi_2Te_3 and Sb_2Te_3, respectively, under optimal electron doping. We notice that the power factor for unstrained Sb_2Te_3 is monotonically increasing for electron carrier concentrations of $N \sim 6$–30×10^{19} cm^{-3}. This behavior can be linked to a deviation of $S_\parallel$ from the Pisarenko relation under electron doping. While it is expected that the thermopower will decrease for increasing carrier concentration, $S_\parallel$ was found to be almost constant in an electron doping range of $N \sim 6$–30×10^{19} cm^{-3} [see Fig. 5(d)]. For the investigated electron doping range of $N \sim 6$–30×10^{19} cm^{-3}, the chemical potential μ at 300 K is located around 300–450 meV above the VBM. As can be seen from the band structure for unstrained Sb_2Te_3 in Fig. 1(b) (black, solid lines), flat nonparabolic bands near the high-symmetry point Z dominate in this energy region and most likely lead to an increased thermopower. This feature is more pronounced for unstrained Sb_2Te_3 than for strained Sb_2Te_3 [red, dashed lines in Fig. 1(b)]. Similar statements can be done for strained and unstrained Bi_2Te_3 [see Fig. 1(a)]. We note, even though this picture is convincing, that it is

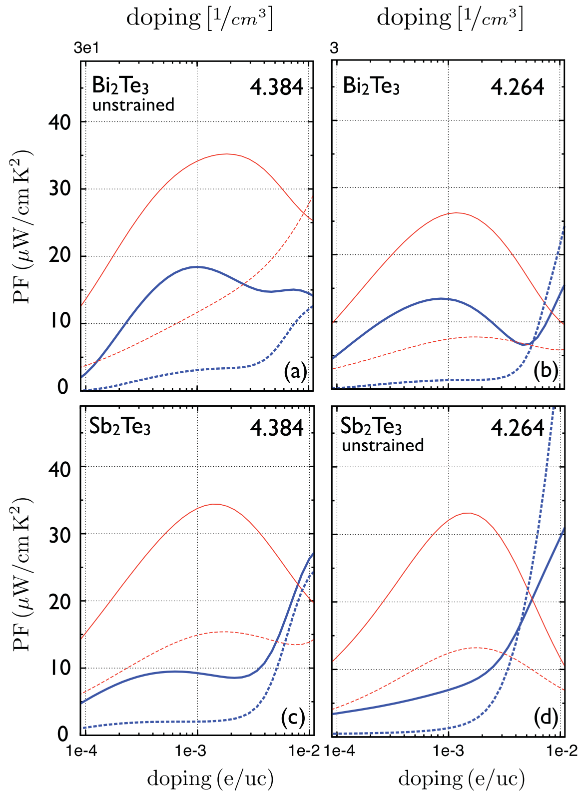

FIG. 7. (Color online) In-plane (solid lines) and cross-plane (dashed lines) doping-dependent power factor at 300 K for (a) Bi_2Te_3 in the Bi_2Te_3, (b) Bi_2Te_3 in the Sb_2Te_3, (c) Sb_2Te_3 in the Bi_2Te_3, and (d) Sb_2Te_3 in the Sb_2Te_3 structures. Electron (hole) doping is presented as blue thick (red thin) line. The charge carrier concentration is stated in units of electron per unit cell (e/uc) ($1/cm^3$) at the bottom (top) x axis.

difficult to link such specific anomalies to the band structure on high-symmetry lines, as the underlying TDF is an integral quantity over all occupied states in the BZ.

Under applied in-plane compressive strain for Bi_2Te_3 [see Fig. 7(b)] and tensile strain for Sb_2Te_3 [see Fig. 7(c)] the obtained changes in the power factor are noticeably different for both tellurides. While for Bi_2Te_3 a decrease of the maximal power factor $PF_{\parallel}$ of about 27% and 23% for n and p doping, respectively, was found, the strain shows nearly no influence on the power factor for Sb_2Te_3. At a carrier concentration of about $N \sim 3 \times 10^{19}$ cm^{-3}, the decrease in $PF_{\parallel}$ for Bi_2Te_3 is about 17% and 28% for n and p doping, respectively, while in the work of Park *et al.*,[14] a slight increase of $PF_{\parallel}$ under strain and hole doping is reported. Obviously, this tendency has to be understood by analyzing the constituent parts $\sigma_{\parallel}$ and $S_{\parallel}$. For compressively strained Bi_2Te_3, at a hole carrier concentration of about $N \sim 3 \times 10^{19}$ cm^{-3}, the electrical conductivity decreases by about 39% to 330 $(\Omega\,\text{cm}\,\text{s})^{-1}$. At the same time, $S_{\parallel}$ increases by about 9%, as shown in Fig. 6(a). This results in the overall decrease of about 28% for $PF_{\parallel}$. Under electron doping of $N \sim 3 \times 10^{19}$ cm^{-3}, no influence of strain could be found for $S_{\parallel}$ at room temperature [see solid blue lines in Fig. 6(a)]. Thus the decrease of $PF_{\parallel}$ under electron doping can be largely related to a decrease of the electrical conductivity under applied compressive strain. By detailed evaluation of the effective mass eigenvalues and eigenvectors, we found a decrease of about 15% for the in-plane electrical conductivity of Bi_2Te_3 under applied strain in the low-temperature and low-doping limit.[22,37] The discussion can be made in the same manner for Sb_2Te_3.[22,37] The fact that strain-induced effects in σ and S tend to compensate each other was already reported for the case of silicon.[25]

As mentioned before (summarized in Figs. 3 and 4), we found a strong anisotropy in the electrical conductivity with $\sigma_{\parallel}/\sigma_{\perp} \gg 1$. The clearly preferred in-plane transport in both bulk tellurides is also reflected in the cross-plane power factor $PF_{\perp}$ (dashed lines in Fig. 7), which is clearly suppressed for all strain states. It is obvious that $PF_{\perp}$ is more suppressed for electron than for hole doping.

Nonetheless, we want to include experimental findings for the thermal conductivity to our calculations, to give an estimation for the figure of merit ZT in plane and cross plane. In Ref. 49, $\kappa_{\parallel} = 2.2$ W/m K, $\kappa_{\perp} = 1.0$ W/m K and $\kappa_{\parallel} = 7.5$ W/m K, $\kappa_{\perp} = 1.6$ W/m K for unstrained Bi_2Te_3 and Sb_2Te_3 are given, respectively. With this, we find maximal values for the figure of merit at room temperature and optimal hole doping of $ZT_{\parallel} \sim 0.48$ and $ZT_{\perp} \sim 0.41$ for unstrained Bi_2Te_3 and $ZT_{\parallel} \sim 0.13$ and $ZT_{\perp} \sim 0.23$ for unstrained Sb_2Te_3. We note that the figure of merit ZT maximizes at slightly lower carrier concentration than the power factor σS^2 shown in Fig. 7. This can be linked directly to an increasing electronic part of the thermal conductivity κ_{el} with increasing carrier concentration.[25,53]

V. CONCLUSION

In the present paper, the influence of in-plane strain on the thermoelectric transport properties of Bi_2Te_3 and Sb_2Te_3 is investigated. A focused view on the influence of strain on the anisotropy of the electrical conductivity σ, thermopower S, and the related power factor σS^2 could help to understand in-plane and cross-plane thermoelectric transport in nanostructured Bi_2Te_3/Sb_2Te_3 superlattices. Based on detailed *ab initio* calculations, we focused mainly on band structure effects and their influence on the thermoelectric transport. For both tellurides, no reasonable decrease of the anisotropy for σ and S could be found under strain, while, in principle, the anisotropy for σ and S is more pronounced under electron doping than at hole doping. Thus a favored thermoelectric transport along the z direction of Bi_2Te_3/Sb_2Te_3 heterostructures due to superlattice-induced in-plane strain effects can be ruled out and a clear preference of p-type thermoelectric transport can be stated for Bi_2Te_3, Sb_2Te_3, and their related epitaxial heterostructures. The absolute value of the in-plane thermopower $S_{\parallel}$ was increased under reduced cell volume, which is in contrast to recent findings by Park *et al.*[14]

We found that even if thermopower or electrical conductivity are enhanced or decreased via applied strain, they tend to compensate each other suppressing more distinct changes of the power factor under strain. We found the thermoelectrically optimal doping to be in the range of $N \sim 3$–6×10^{19} cm^{-3} for all considered systems. Our assumption of an anisotropic relaxation time for Bi_2Te_3, states that already in the single crystalline system, strong anisotropic scattering effects should play a role.

ACKNOWLEDGMENTS

This work was supported by the Deutsche Forschungsgemeinschaft, SPP 1386 "Nanostrukturierte Thermoelektrika: Theorie, Modellsysteme und kontrollierte Synthese." N. F. Hinsche is member of the International Max Planck Research School for Science and Technology of Nanostructures.

*nicki.hinsche@physik.uni-halle.de

[1] B. Sales, Science **295**, 1248 (2002).
[2] A. Majumdar, Science **303**, 777 (2004).
[3] H. Böttner, G. Chen, and R. Venkatasubramanian, MRS Bull. **31**, 211 (2006).
[4] H. Goldsmid, A. Sheard, and D. Wright, Br. J. Appl. Phys. **9**, 365 (1958).
[5] R. Venkatasubramanian, E. Siivola, and T. Colpitts, Nature (London) **413**, 597 (2001).
[6] R. Venkatasubramanian, T. Colpitts, B. O'Quinn, S. Liu, N. El-Masry, and M. Lamvik, Appl. Phys. Lett. **75**, 1104 (1999).
[7] R. Venkatasubramanian, Phys. Rev. B **61**, 3091 (2000).
[8] H. Beyer, J. Nurnus, H. Böttner, A. Lambrecht, E. Wagner, and G. Bauer, Physica E: Low-dimensional Systems and Nanostructures **13**, 965 (2002).
[9] H. Böttner, J. Nurnus, A. Gavrikov, and G. Kuhner, J. Microelectromech. Syst. **13**, 414 (2004).
[10] J. König, M. Winkler, S. Buller, W. Bensch, U. Schürmann, L. Kienle, and H. Böttner, J. Electron. Mater. **40**, 1266 (2011).
[11] C.-N. Liao, C.-Y. Chang, and H.-S. Chu, J. Appl. Phys. **107**, 066103 (2010).
[12] N. Peranio, O. Eibl, and J. Nurnus, J. Appl. Phys. **100**, 114306 (2006).
[13] M. N. Touzelbaev, P. Zhou, R. Venkatasubramanian, and K. E. Goodson, J. Appl. Phys. **90**, 763 (2001).
[14] M. S. Park, J.-H. Song, J. E. Medvedeva, M. Kim, I. G. Kim, and A. J. Freeman, Phys. Rev. B **81**, 155211 (2010).
[15] H. Li, D. Bilc, and S. D. Mahanti, Mat. Res. Soc. Symp. Proc. **793**, 837 (2004).
[16] T. Scheidemantel, C. Ambrosch-Draxl, T. Thonhauser, J. V. Badding, and J. Sofo, Phys. Rev. B **68**, 125210 (2003).
[17] T. Thonhauser, T. Scheidemantel, J. O. Sofo, J. Badding, and G. Mahan, Phys. Rev. B **68**, 085201 (2003).
[18] B.-L. Huang and M. Kaviany, Phys. Rev. B **77**, 125209 (2008).
[19] *Landolt-Börnstein New Series, group III/41C* (Springer Verlag, Berlin, 1998).
[20] M. Gradhand, M. Czerner, D. V. Fedorov, P. Zahn, B. Y. Yavorsky, L. Szunyogh, and I. Mertig, Phys. Rev. B **80**, 224413 (2009).
[21] S. H. Vosko and L. Wilk, Phys. Rev. B **22**, 3812 (1980).
[22] P. Zahn, N. F. Hinsche, B. Y. Yavorsky, and I. Mertig, e-print arXiv:1108.0023 (unpublished).
[23] I. Mertig, Rep. Prog. Phys. **62**, 237 (1999).
[24] P. Zahn, I. Mertig, M. Richter, and H. Eschrig, Phys. Rev. Lett. **75**, 2996 (1995).
[25] N. F. Hinsche, I. Mertig, and P. Zahn, J. Phys. Condens. Matter **23**, 295502 (2011).
[26] T. Vojta, I. Mertig, and R. Zeller, Phys. Rev. B **46**, 15761 (1992).
[27] J. Yang, H. Li, T. Wu, and W. Zhang, Adv. Funct. Mater. **18**, 2880 (2008).
[28] J. Barth, G. H. Fecher, B. Balke, S. Ouardi, T. Graf, C. Felser, A. Shkabko, A. Weidenkaff, P. Klaer, and H. Elmers, Phys. Rev. B **81**, 064404 (2010).
[29] D. J. Singh, Phys. Rev. B **81**, 195217 (2010).
[30] D. Parker and D. J. Singh, Phys. Rev. B **82**, 035204 (2010).
[31] A. F. May, D. J. Singh, and G. J. Snyder, Phys. Rev. B **79**, 153101 (2009).
[32] M.-S. Lee, F. Poudeu, and S. D. Mahanti, Phys. Rev. B **83**, 085204 (2011).
[33] S. Lee and P. von Allmen, Appl. Phys. Lett. **88**, 022107 (2006).
[34] M. Situmorang and H. Goldsmid, Phys. Status Solidi B **134**, K83 (1986).
[35] T. Thonhauser, Solid State Commun. **129**, 249 (2004).
[36] G. Mahan and J. Sofo, Proc. Natl. Acad. Sci. USA **93**, 7436 (1996).
[37] B. Y. Yavorsky, N. F. Hinsche, I. Mertig, and P. Zahn, e-print arXiv:1109.0186 (unpublished).
[38] D. M. Rowe, *CRC Handbook of Thermoelectrics* (CRC, London, 1995).
[39] R. Delves, A. Bowley, and D. Hazelden, Proceedings of the Phys. Society **78**, 838 (1961).
[40] H. Jeon, H. Ha, D. Hyun, and J. Shim, J. Phys. Chem. Solids **52**, 579 (1991).
[41] H. Kaibe, J. Phys. Chem. Solids **50**, 945 (1989).
[42] M. Stordeur and W. Kühnberger, Phys. Status Solidi B **69**, 377 (1975).
[43] M. Stordeur and W. Heiliger, Phys. Status Solidi B **78**, K103 (1976).
[44] M. Zhitinskaya, V. Kaidanov, and V. Kondratev, Sov. Phys. Semicond. **10**, 1300 (1976).
[45] E. Müller, *Bandstruktur und Ladungsträgerstreuung in p-leitenden* $(Bi_{1-x}Sb_x)_2Te_3$*-Mischkristallen* (VDI Verlag, Düsseldorf, 1998).
[46] M. Cutler and N. Mott, Phys. Rev. **181**, 1336 (1969).
[47] G. Simon and W. Eichler, Phys. Status Solidi B **103**, 289 (1981).
[48] H. Langhammer, M. Stordeur, H. Sobotta, and V. Riede, Phys. Status Solidi B **109**, 673 (1982).
[49] A. Jacquot, N. Farag, M. Jaegle, M. Bobeth, J. Schmidt, D. Ebling, and H. Böttner, J. Electron. Mater. **39**, 1861 (2010).
[50] S. Cho, Y. Kim, A. Divenere, G. K. Wong, J. B. Ketterson, and J. R. Meyer, Appl. Phys. Lett. **75**, 1401 (1999).
[51] J. Nurnus, Ph.D. thesis, Albert-Ludwigs-Universität Freiburg, 2001.
[52] A. F. Ioffe, *Physics of Semiconductors* (Academic, New York, 1960).
[53] G. J. Snyder and E. Toberer, Nat. Mater. **7**, 105 (2008).